Remote sensing of cirrus cloud properties in the presence of lower clouds: An ATSR-2 case study during the Interhemispheric Differences in Cirrus Properties From Anthropogenic Emissions (INCA) experiment

Albano González, Peter Wendling, Bernhard Mayer, Jean-François Gayet, Tom Rother

Remote sensing of cirrus cloud properties in the presence of lower clouds: An ATSR-2 case study during the Interhemispheric Differences in Cirrus Properties From Anthropogenic Emissions (INCA) experiment

Albano González,[1,5] Peter Wendling,[2] Bernhard Mayer,[2] Jean-Francois Gayet,[3] and Tom Rother[4]

[1]   The retrieval of cirrus cloud microphysical properties in a multilayer cloud system is a challenge due to the usually low optical thickness of the ice cloud under investigation. However, it is estimated that about 50% of all cirrus clouds occur in such multilayer systems. Here, we present a method that uses a combination of five observations by the dual-view ATSR-2 radiometer onboard the ERS-2 satellite. Using the channels at 0.87 and 1.6 μm in both nadir and forward views and the nadir view of the 3.7 μm band, the retrieval can clearly separate a thin high cloud from a highly reflective low water cloud and thus determine the optical thickness and effective particle size of the cirrus quantitatively. This is confirmed by a comparison of the retrieved parameters with in situ aircraft observations made on 23 March 2000 near Punta Arenas, Chile, where good agreement was observed. An important finding of this study was that the pixel-to-pixel variability of the low cloud cannot be neglected. In other words, the optical thickness of the low cloud needs to be included as a retrieval parameter, because the assumption of constant optical properties leads to large degree of uncertainties in the derived ice cloud parameters.   INDEX TERMS: 0320 Atmospheric Composition and Structure: Cloud physics and chemistry; 3359 Meteorology and Atmospheric Dynamics: Radiative processes; 3360 Meteorology and Atmospheric Dynamics: Remote sensing; KEYWORDS: multilayer cirrus, ATSR-2, remote sensing

Citation: González, A., P. Wendling, B. Mayer, J.-F. Gayet, and T. Rother, Remote sensing of cirrus cloud properties in the presence of lower clouds: An ATSR-2 case study during the Interhemispheric Differences in Cirrus Properties From Anthropogenic Emissions (INCA) experiment, *J. Geophys. Res.*, *107*(D23), 4693, doi:10.1029/2002JD002535, 2002.

1.   Introduction

[2]   Cirrus clouds significantly influence the Earth−ocean−atmosphere energy balance because of their large spatial and temporal coverage and their low temperatures, affecting both the incoming solar radiation and the outgoing thermal radiation [*Ramanathan et al.*, 1989]. Moreover, they have been identified as one of the most important but yet not fully understood components in atmospheric research [*Liou*, 1986; *Stephens et al.*, 1990; *Liou*, 1992]. Whether cirrus clouds tend to cool or heat the Earth depends on their radiative properties, which in turn are determined by their composition and their vertical position. Intensive field experiments have been carried out during the last two decades in order to improve our understanding of this topic, for example, FIRE I and II in 1986 and 1991, respectively [*Starr*, 1987; *Arnott et al.*, 1994; *Mitchell and Arnott*, 1994], ICE'89 [*Raschke et al.*, 1990] and EUCREX'94 [*Sauvage et al.*, 1999]. The data used in the present study were acquired during the Interhemispheric Differences in Cirrus Properties From Anthropogenic Emissions (INCA) experiment [*Ström et al.*, 2001] which was funded within the European Union Fifth Frame Work Programme.

[3]   The determination of cirrus properties on a larger scale requires the use of satellite data. Numerous approaches, based on the interpretation of the radiation reflected or emitted by cirrus clouds in different bands of the electromagnetic spectrum, have been developed to infer cloud optical thickness and mean effective ice crystal size from radiances measured by satellite borne radiometers [see, e.g., *Ou et al.*, 1993; *King et al.*, 1997; *Ou et al.*, 1999; *Rolland et al.*, 2000]. Nevertheless, despite the fact that surface and aircraft observations show that multiple cloud layers occur in about a half of all cloud observations, often associated with frontal areas [*Tian and Curry*, 1989; *Mace et al.*, 1997], most of these satellite cirrus cloud retrieval techniques have been designed for single-layer cloud systems. The application of

---

[1]Dpto. Física, Universidad de La Laguna, La Laguna, Spain.
[2]Institut für Physik der Atmosphäre, Deutsches Zentrum für Luft- und Raumfahrt, Oberpfaffenhofen, Wessling, Germany.
[3]Laboratoire de Météorologie Physique, Université Blaise Pascal, Clermont-Ferrand, France.
[4]Institut für Methoden der Fernerkundung, Deutsches Zentrum für Luft- und Raumfahrt, Oberpfaffenhofen, Wessling, Germany.
[5]During this work at Institut für Physik der Atmosphäre, DLR, Oberpfaffenhofen, Germany.

these approaches to multilayer conditions leads to erroneous results. For this reason, several schemes have been developed to identify multilayer clouds [e.g., *Baum et al.*, 1995; *Ou et al.*, 1996; *Baum et al.*, 1997; *Baum and Spinhirne*, 2000]. Few studies aimed at the retrieval of multilayer cloud parameters [*Baum et al.*, 1994, 1995; *Ou et al.*, 1998]. The majority of these approximations have been developed for single-view instruments, such as the Advanced Very High Resolution Radiometer (AVHRR) or the Moderate Resolution Imaging Spectroradiometer (MODIS). In these cases, a specific crystal habit (particle shape) must be assumed a priori [*Baran et al.*, 1999b], and all retrievals will be sensitive to this assumption [*Mishchenko et al.*, 1996; *Rolland et al.*, 2000]. Only with the help of dual- or multiple-view instruments, like the Along Track Scanning Radiometer (ATSR) or the Multiangle Imaging Spectroradiometer (MISR), is it possible to estimate the dominant ice particle shape. *Baran et al.* [1999a, 1999b] and *Knap et al.* [1999], for example, studied the applicability of ATSR-2 data for the retrieval of bulk and microphysical cloud properties in single-layer cases.

[4] Here we demonstrate the possibility of retrieving cirrus cloud optical thickness and effective crystal size from ATSR-2 data under extreme conditions, that is, for an optically thin cirrus layer over a variable low water cloud. The retrieval results are compared to in situ aircraft observations carried out on 23 March 2000 in Punta Arenas, Chile. Section 2 gives an overview of the aircraft and satellite instruments and the data used in this case study. Section 3 describes the radiative transfer model used to simulate the satellite radiances and the parameterization of the single scattering properties of the ice crystals. A comparison between the phase functions measured by a polar nephelometer [*Gayet et al.*, 1997; *Crépel et al.*, 1997] and the theoretical ones demonstrates the applicability of the parameterization used. Section 4 presents the retrieval scheme used to obtain the cirrus parameters from ATSR-2 radiances and a corresponding uncertainty analysis is shown in section 5. A comparison between in situ measurements and retrieved parameters for the selected case study is discussed in section 6. Finally, summary and conclusions are presented in section 7.

2. Instrumentation and Measurements

[5] The observations presented in this study were obtained on 23 March 2000 near Punta Arenas, Chile, during the European INCA experiment. We selected this particular day because of the availability of coincident in situ microphysical observations and ATSR-2 satellite data during multilayer cloud conditions. In the following subsections the instruments and data used in this study will be described.

2.1. Aircraft Measurements

[6] During the INCA campaign, in situ data were obtained from four instruments onboard the German research aircraft Falcon, which is operated by Deutsches Zentrum für Luft- und Raumfahrt (DLR) (J. F. Gayet et al., Quantitative measurements of the physical and optical properties of cirrus clouds with four different in situ probes: Evidence of small crystals, submitted to *Journal of Geophysical Research*, 2002). In this study the microphysical

and optical cloud parameters were inferred from measurements of the PMS FSSP-300 optical particle counter [*Baumgardner et al.*, 1992] for particles of diameter 0.3 to 15.8 µm, the PMS 2D-C probe [*Knollenberg*, 1981; *Gayet et al.*, 1996] for the size range from 25 to 800 µm, and the polar nephelometer for the scattering phase function [*Gayet et al.*, 1997; *Auriol et al.*, 2001]. In addition, the Falcon was equipped with meteorological and navigation instruments.

[7] The cloud microphysical parameters have been obtained using the following relations for effective diameter (D_{eff}), ice water content (IWC) and extinction coefficient (σ_{ext})

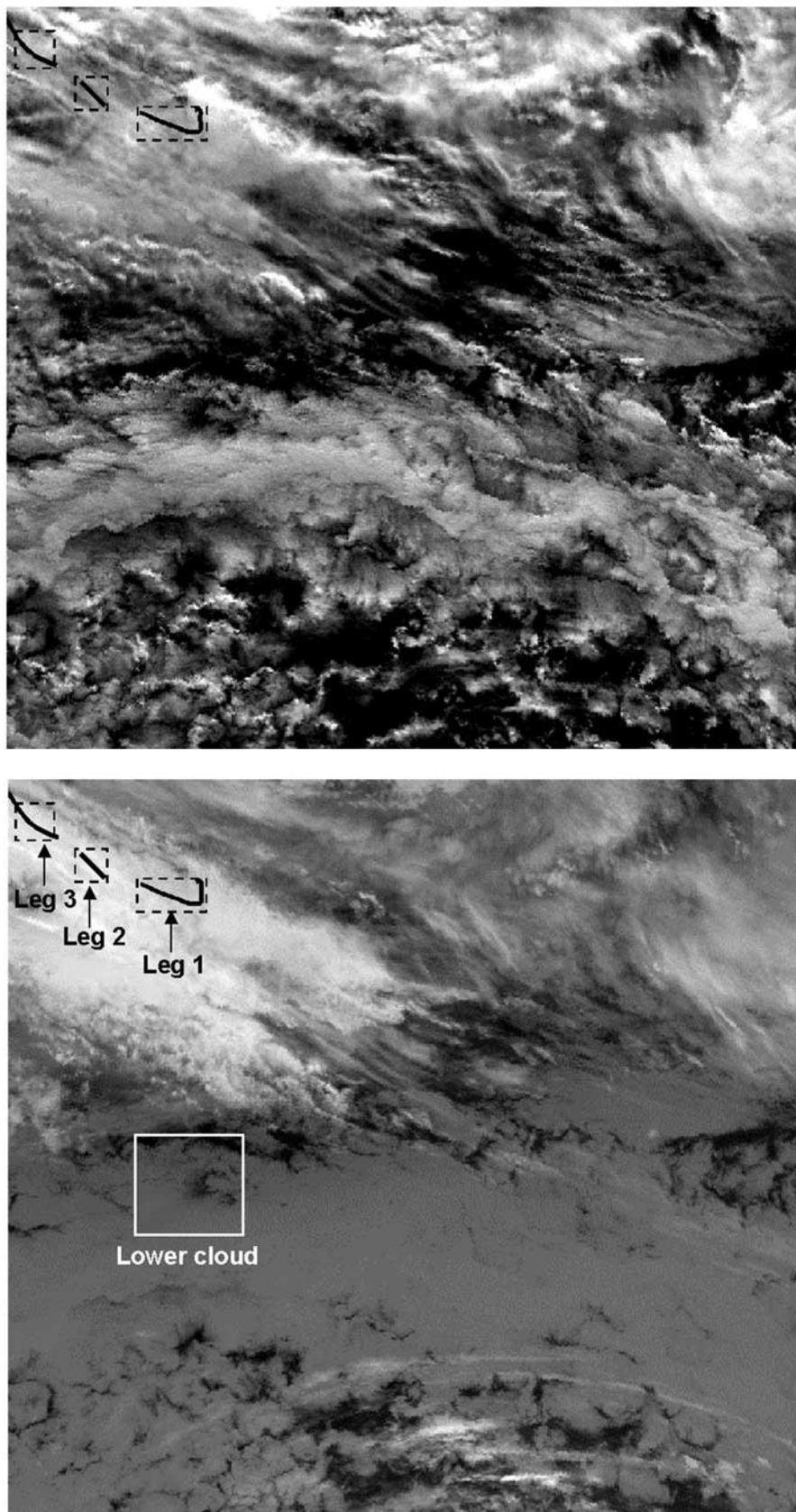$$D_{eff} = \frac{2 \sum_{i=1}^{n} N_i \left(\frac{1}{2} D_i^{melt}\right)^3}{\sum_{i=1}^{n} N_i A_i / \pi} \tag{1}$$

$$IWC = \frac{\pi}{6} \rho_w \sum_{i=1}^{n} N_i \left(D_i^{melt}\right)^3 \tag{2}$$
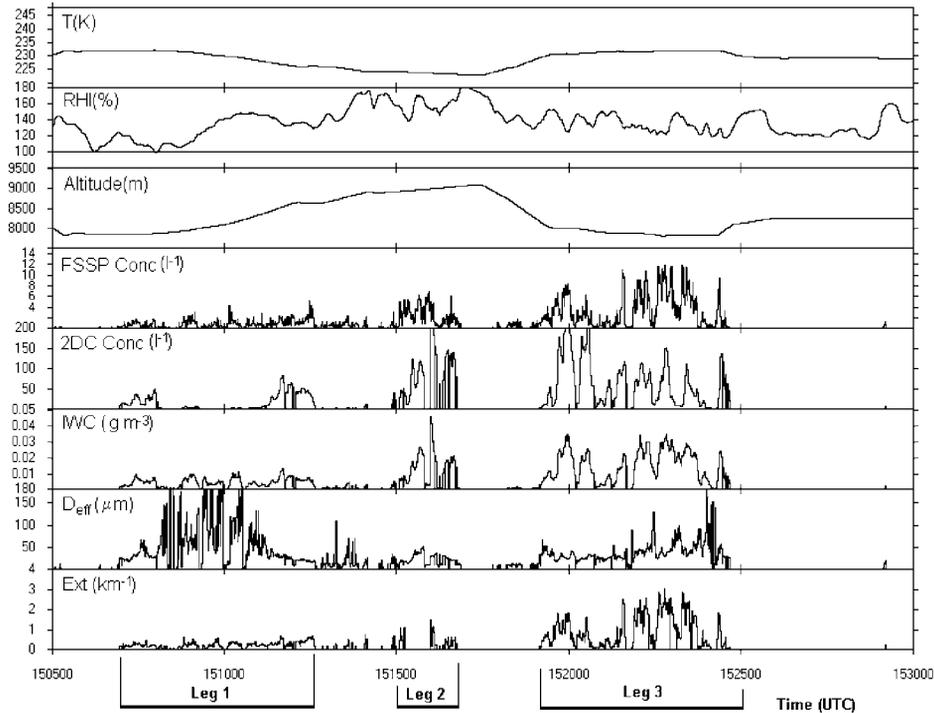
$$\sigma_{ext} = \sum_{i=1}^{n} Q_{ext}^i N_i A_i \tag{3}$$

where D_i^{melt} is the equivalent melted diameter, N_i is the size spectrum as a function of the particle area A_i, ρ_w is the water density and Q_{ext}^i is the visible extinction efficiency, assumed to have a value equal to 2 (large ice particle approximation). The equivalent melted diameter was obtained from the projected surface of the ice particle using the relationships suggested by *Heymsfield* [1972] for small irregular particles and *Locatelli and Hobbs* [1979] for larger irregular particles.

[8] The selected flight track was located over the Pacific Ocean, near the coast of Chile. One part of this track was almost completely within a cirrus cloud, and ascents and descents through the cloud layer were performed. The aircraft trajectory started at 15:07UTC around (55°S, 71°W) and finished at 15:25UTC around (54°S, 74°W). It was divided into three unconnected legs that correspond to different ambient conditions and altitudes. The three flight legs are presented in Figure 1 superimposed on the ATSR-2 images which are explained in the next section.

[9] Figure 2 depicts the time series of the microphysical and optical cloud parameters and Figure 3 shows the particle size distributions averaged over each of the three legs. On the first leg the Falcon flew at constant altitude, near the cloud base, for some minutes and then started to ascend. The concentration of small particles is low and the relative humidity with respect to ice (RHI) is near 100%. Hence, leg 1 is probably a decaying or relaxing cirrus with size sorting where the smallest particles are found near the top of the cirrus layer, becoming larger towards cloud base. These results are in general agreement with previous studies of cirrus clouds [*McFarquhar and Heymsfield*, 1997; *Yang et al.*, 2001]. The second leg corresponds to an optically thicker forming cloud, where high supersaturation over ice and a rather large concentration of small particles were observed. Despite the lower sample level during leg 3, the cloud appears to be still forming and optically thick. The

Figure 1. ATSR-2 0.87 (a) and 10.8 μm (b) channel images of the selected region, Pacific Ocean near Punta Arenas, Chile, on 23 March 2000. Leg 1, leg 2 and leg 3 denote the flight legs carried out with the research aircraft Falcon.

Figure 2. Time series of the microphysical and optical cirrus cloud parameters for the three studied flight legs: ambient temperature, relative humidity with respect to ice, altitude, ice particle size and concentration as well as mean effective particle size and total ice water content from the FSSP and 2D-C probe, and extinction coefficient from the polar nephelometer.

mean values for the obtained ice cloud parameters are summarized in Table 1.

2.2. ATSR-2 Data

[10] The Along Track Scanning Radiometer (ATSR-2) onboard the European Remote Sensing Satellite (ERS-2) has seven spectral bands centered at the wavelengths 0.55, 0.67, 0.87, 1.6, 3.7, 10.8 and 11.9 μm. It has been designed to observe the same scene in near-nadir (zenith angle between 0 and 22°) and forward (52–55°) views using a conical scanning geometry [*Prata et al.*, 1990]. The forward image is measured approximately two minutes before the nadir image. The spatial resolution at the subsatellite point is about 1 km while the pixel size is about 3–4 km for forward view. Data are supplied to users geolocated to a grid of 1 km pixels, where forward and nadir images are coincident. To correct for the effects of parallax and cloud drift, nadir and forward images have to be reregistered with regard to the cloud top [*Knap et al.*, 1999]. However, automatic methods based on cross correlation between the two images present some problems for thin cirrus overlying water clouds [*Baran et al.*, 1999a]. Consequently, in our case this process was carried out by shifting the images by visual inspection.

[11] The region used for our study is shown in Figure 1, in particular, the 0.87 and 10.8 μm nadir images. This observation was made by ATSR-2 around 30 minutes before the in situ measurements. It shows a large area covered by a broken low cloud layer, which in some parts, like in our study area, is overlaid by an optically thin
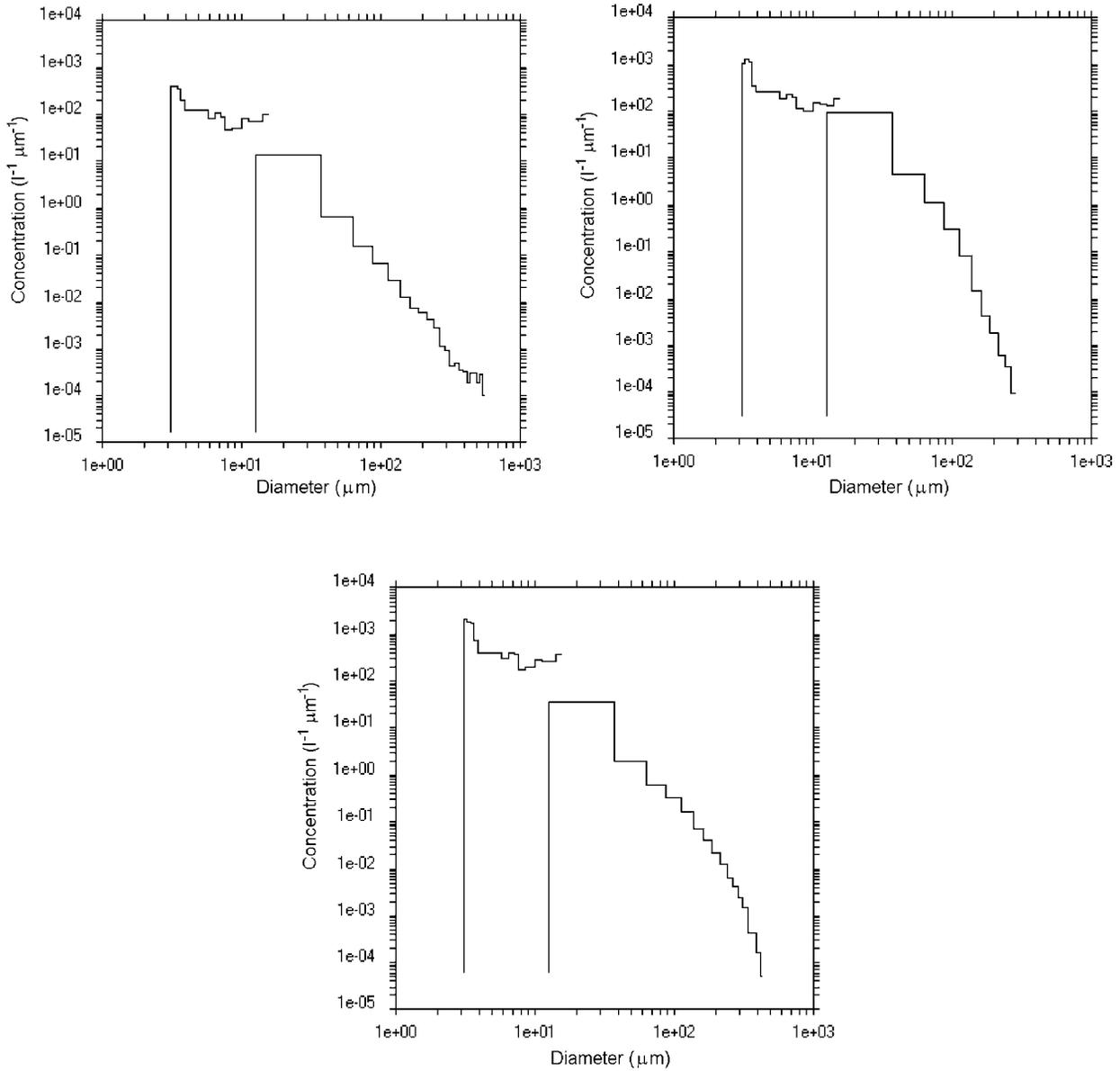
cirrus layer. The dashed line boxes in Figure 1 surrounding the flight legs correspond to the regions used in the following to retrieve the cirrus parameters from satellite data.

3. Model Description

[12] The radiative properties of cirrus clouds are determined by the concentration, shape and size distribution of the ice crystals and their spatial distribution. Therefore, the retrieval of cloud parameters from satellite data requires a detailed model of both single and multiple scattering properties of clouds.

3.1. Single Scattering Properties of Ice Crystals

[13] Cirrus clouds are composed of mostly nonspherical ice particles with various shapes and sizes, as has been demonstrated by multiple in situ observations [e.g., *Heymsfield and Platt*, 1984; *McFarquhar et al.*, 1999]. This feature must be accounted for in the development of a reliable satellite retrieval algorithm because the scattering phase function of spherical particles is systematically different from that of nonspherical particles and hence the spherical approximation is inadequate to represent scattering and absorption properties of ice crystals [*Takano and Liou*, 1989; *Fu et al.*, 1999]. Here we have used the parameterization by *Key et al.* [2002] for the shortwave and near infrared (0.2–5.0 μm) optical properties of ice clouds for a variety of particle shapes (habits). It provides the volume extinction coefficient (β_e), the single scattering
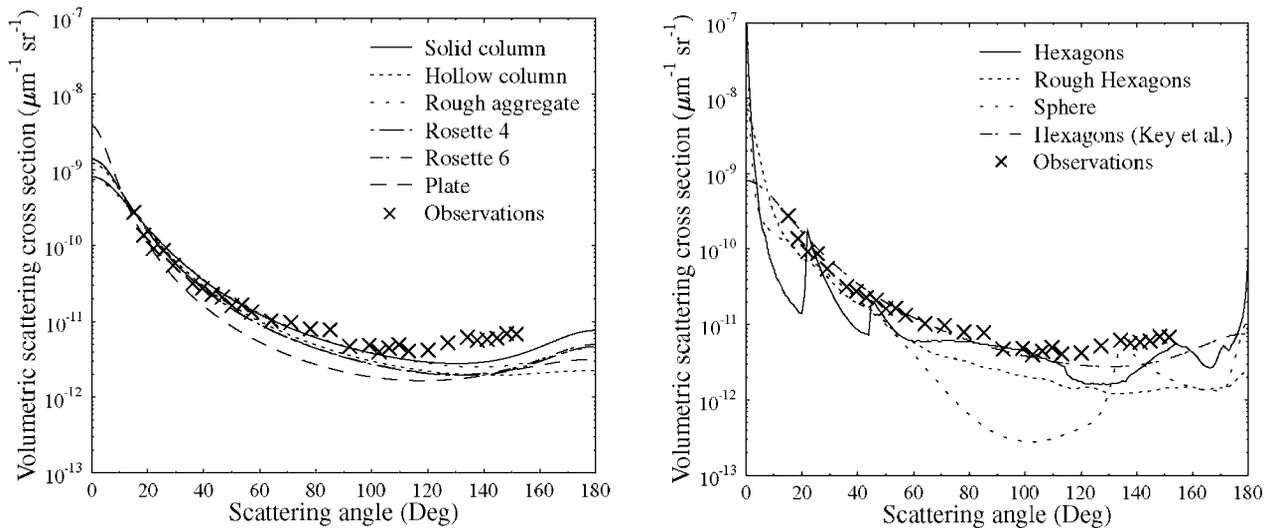
Figure 3.   Average ice crystal size distribution measured by the PMS FSSP-300 and the 2D-C probes for a) leg 1, b) leg 2 and c) leg 3.

albedo (ω) and the asymmetry parameter (g) as a function of crystal effective size and ice water content IWC for six different habits and 56 spectral bands. These relationships were obtained by integrating the single scattering properties for individual crystals [*Yang et al.*, 2000] over 30 observed size distributions from midlatitude and tropical cirrus clouds. The habits are hexagonal solid and hollow columns, hexagonal plates, two- and three-dimensional rosettes (with four and six branches respectively) and rough aggregates of columns.

Table 1.   Falcon Observation of Mean Concentration, Ice Water Content, Effective Crystal Size, Extinction Coefficient, Asymmetry Parameter, and Associated Standard Deviations (in Parentheses) for the Three Legs Used in this Study

	Concentration, cm^{-3}	IWC, g/m^3	$D_{\text{eff},i}$, μm	Extinction Coefficient, km^{-1}	Asymmetry Parameter
Leg 1	0.8 (0.7)	0.005 (0.003)	55 (35)	0.25 (0.12)	0.771 (0.006)
Leg 2	2.1 (1.5)	0.011 (0.007)	34 (12)	0.50 (0.30)	0.786 (0.004)
Leg 3	3.9 (2.9)	0.020 (0.010)	47 (20)	1.10 (0.70)	0.773 (0.005)

Figure 4. Comparison between volumetric scattering cross sections measured by the polar nephelometer for leg 1 and the parameterization by *Key et al.* [2002] for six different habits (a) and theoretical results for hexagonal ice columns with smooth and rough surfaces (b).

[14] Often the Henyey-Greenstein (HG) phase function is used as an approximation of the scattering phase function:

$$P_{HG}(\theta; g) = \frac{1 - g^2}{(1 + g^2 - 2g \cos \theta)^{3/2}} \tag{4}$$

where g is the asymmetry parameter and θ is the scattering angle. However, this approximation does not reproduce the backscattering behavior properly. For this reason, *Key et al.* [2002] used a double Henyey-Greenstein function

$$P_{dHG}(\theta) = f P_{HG}(\theta; g_1) + (1 - f) P_{HG}(\theta; g_2) \tag{5}$$

where g_1 describes the forward scattering, g_2 accounts for the backscattering peak and f is a number between 0 and 1.

[15] As mentioned in the previous section, the Falcon carried a polar nephelometer, which measures the scattering phase function (from $\pm3.5°$ to $\pm169°$) of an ensemble of cloud particles that intersect a collimated laser beam at a wavelength of 0.8 μm [*Gayet et al.*, 1997]. Figure 4a shows a comparison of the observed volumetric scattering phase function with the data of *Key et al.* [2002] for the six habits. The crosses represent the averaged polar nephelometer measurements averaged over leg 1 and the curves are the *Key et al.* [2002] results for the observed effective particle size and ice water content, see Table 1. The most noticeable features are the smooth shape of the measured volumetric scattering cross-section and the absence of the 22° and 46° halos which are typical for hexagonal shapes. These measurements agree with previous results [e.g., *Volkovitskiy et al.*, 1980; *Doutriaux-Boucher et al.*, 2000]. The selected parameterization represents forward scattering reasonably well but it fails to explain the backscattering behavior. These discrepancies could possibly be attributed to a contamination of the measurement signal by stray light in the backward direction [*Gayet et al.*, 1998]. The backward direction is critical for the retrieval because the viewing

geometry for ATSR-2 observations at these latitudes causes scattering angles in this range. For example, the mean scattering angles for the box corresponding to leg 1 (Figure 1) are 123.7° and 162.4° for the nadir and forward views respectively.

[16] For comparison purposes, we also calculated the theoretical volumetric scattering cross-sections for smooth and rough hexagonal columns using the particle size distributions measured by the FSSP-300 and 2D-C probes. Scattering properties for particles small compared to the wavelength were calculated with a new method derived from a generalization of the separation variables method for infinitely extended hexagonal cylinders [*Rother*, 1998; *Rother et al.*, 2001]. On the basis of this rigorous approach an approximation to finite hexagonal cylinders is obtained by applying the Huygens principle [*Rother et al.*, 1999]. For large particles with smooth surfaces we used a ray-tracing program for the calculation of the single scattering properties of randomly oriented ice crystals [*Hess and Wiegner*, 1994; *Wendling et al.*, 1979]. Finally, for large particles with rough surfaces the scattering properties were also calculated using a ray-tracing method [*Macke*, 1993; *Macke et al.*, 1996]. Forty-three different crystal sizes from 3.4 to 700 μm were used to compute the single scattering properties, coinciding with the size bins observed by the instruments. For the aspect ratio of hexagonal columns we used empirical relationships between length and diameter reported by *Mitchell and Arnott* [1994]. The volumetric scattering cross-sections calculated for leg 1 are shown in Figure 4b, together with the parameterization for solid hexagonal columns and the computation for spherical particles using Mie theory [*Wiscombe*, 1980]. Again, the theoretical calculations underestimate the observed backscattering. The most striking feature, however, is the large difference between the scattering functions of spherical and nonspherical particles which exceeds one order of magnitude in the sideward direction. In contrast, all parameterizations and calculations for nonspherical particles and the observations are in close

enough agreement to justify the use of the parameterization proposed by *Key et al.* [2002] as being representative of the scattering properties of nonspherical particles.

3.2. Radiative Transfer Computations

[17] The development of a retrieval scheme to extract the macroscopic and microscopic parameters of cirrus clouds from satellite imagery requires a numerical forward model for the calculation of the radiances observed by the satellite instrument. In this study the libRadtran model package [*Kylling and Mayer*, 1993–2002, available at http://www. libradtran.org] was used. For the radiance calculations we used the one-dimensional plane-parallel discrete ordinates method DISORT 2.0 [*Stamnes et al.*, 1988] which is one of several solvers provided by libRadtran. The single scattering properties of ice crystals were calculated using the parameterization by *Key et al.* [2002] described in the previous section. For water clouds we used Mie theory where the droplet size distribution was described by a gamma distribution. Profiles of pressure, temperature, and trace gas concentrations were taken from the midlatitude summer atmosphere compiled by *Anderson et al.* [1986]. Rayleigh scattering was calculated according to *Nicolet* [1984] and molecular absorption was parameterized using the three-term exponential sum fitting technique provided by the SBDART radiative transfer model [*Ricchiazzi et al.*, 1998] which was, for this purpose, interfaced to libRadtran. Homogeneous water and ice clouds with various optical thicknesses and effective particle sizes were added. Their vertical location was defined by their top temperature which was used as a retrieval parameter. As the retrieval was exclusively done over the ocean, the surface reflectivity was taken from the clear water spectral albedo provided by *Viollier* [1980].

[18] Radiances were calculated by dividing each ATSR-2 channel into 15 equally-sized wavelength bands, calculating reflectivities for these bands, interpolating the reflectivities to a 1nm resolution, multiplying with the extraterrestrial irradiance, weighting with the ATSR-2 spectral responses, and integrating over wavelength. For the thermal channels including the 3.7 μm channel, these radiances were converted to brightness temperatures through the inverse of the Plank function using the effective wavenumber for each band, which was calculated for each radiance using the method suggested by *Sospedra et al.* [1998]. Finally, a lookup table of radiances and brightness temperatures was created for a variety of low and high cloud conditions to be used as the basis of the retrieval.
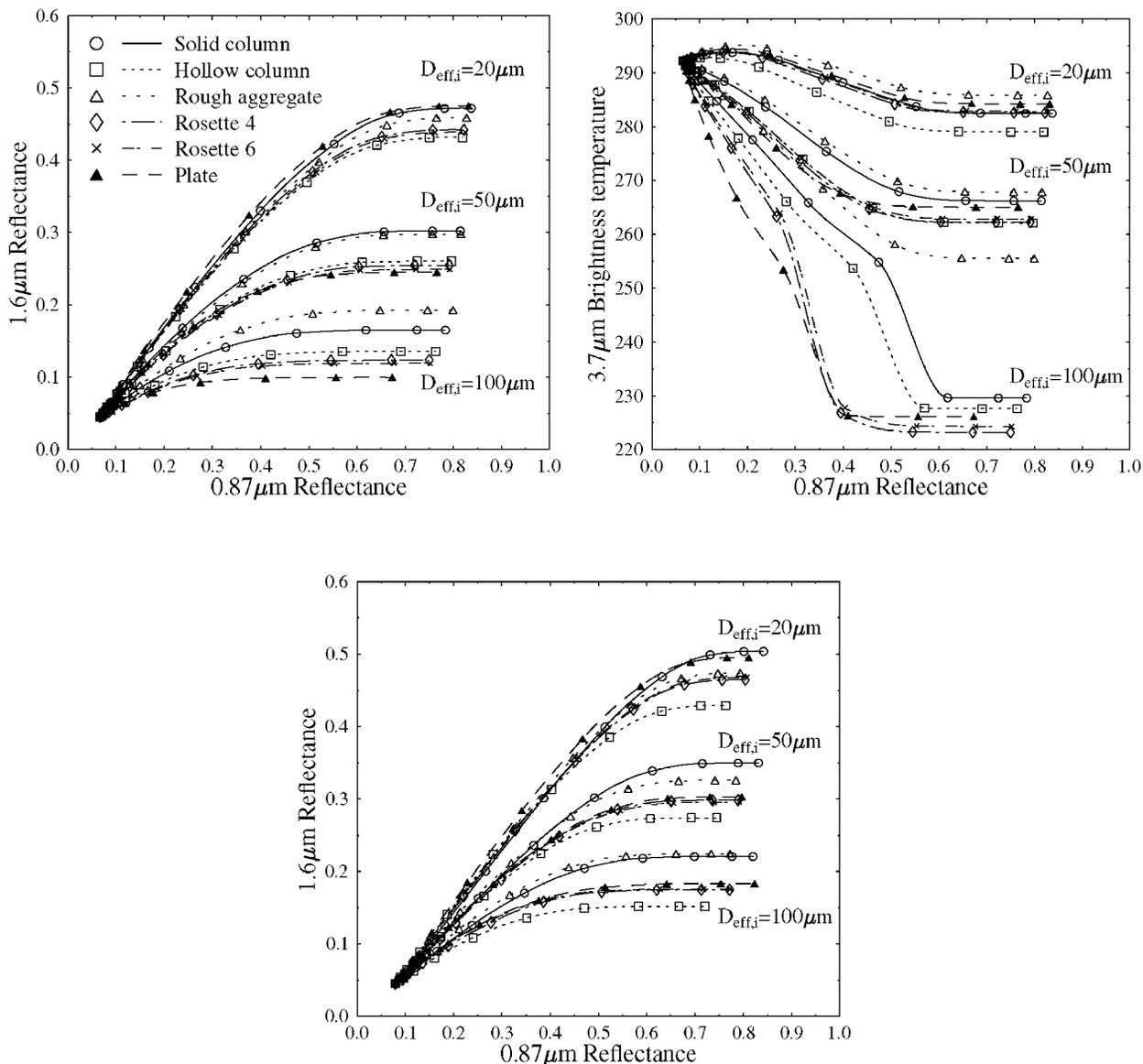
4. Retrieval Method

[19] Our aim is the retrieval of cirrus cloud optical properties, in particular optical thickness, effective diameter and habit. These three parameters could in principle be retrieved from three independent pieces of information, that is, a combination of three ATSR-2 channels. However, as we focused on multilayer clouds, there is at least one further parameter required that determines the reflectivity of the low cloud. Finally it turned out that a fifth parameter is required that helps to really distinguish between high and low cloud which in our case is the cloud top temperature of the high cloud. As we will show in this section, an

appropriate combination of five observations allows us to quantitatively determine the optical properties of the high cloud, even in the presence of a highly reflective low cloud. Here we chose to use the channels at 0.87 and 1.6 μm in both nadir and forward views, and the nadir view of the 3.7 μm band. This selection was done performing multiple theoretical simulations for different cloud conditions and choosing the optimum combination of channels that allowed us to obtain the desired parameters.

[20] Figure 5 shows combinations of selected channels for different ice crystal effective diameters and optical thicknesses. Figure 5a demonstrates the well-known fact that the 0.87 μm radiance depends mostly on optical thickness while the 1.6 μm radiance is also strongly affected by the particle size. A comparison between the nadir and forward views (Figures 5a and 5c) indicates that it might be possible to retrieve the particle habit by combining both viewing directions because the order of the curves for different habits varies between both plots. The particular shape of the curves in Figure 5b, mainly for large ice particles, is due to the fact that the 3.7 μm radiance is the sum of solar and thermal contributions.

[21] Using the correlations for the 0.87 and 1.6 μm channels (Figures 5a and 5c), it is possible to obtain the ice particle size, dominating shape, and optical thickness of a single-layer cirrus cloud. The 3.7 μm channel provides information about cloud top temperature and helps to separate the thin high cloud from the optically thick low cloud. Ocean reflectance and sea surface temperature which are additionally required by the retrieval can be estimated from nearby clear pixels. The situation becomes more complicated when the cirrus is overlapping a lower cloud layer. In this case, the properties of the lower cloud need to be taken into account because the reflection at the lower, usually optically thick, cloud dominates the signal. Figure 6 shows four representative cases for the correlation between ATSR-2 selected channels with different lower cloud conditions. These plots show the importance of including the lower layer properties in the retrieval scheme for optically thin cirrus. Only in the case of optically thick cirrus, the presence of a lower layer does not affect the radiances reaching the sensor.

[22] To account for the lower cloud, the effective radius, optical thickness and top temperature of the low cloud were obtained for a box located near the cirrus cloud (Figure 1b) using the 0.87, 1.6 and 10.8 μm channels in nadir view. The retrieval method was similar to that used for the cirrus properties, as explained below. Figure 7 shows effective radius and optical thickness of the low cloud. A clear correlation between both parameters is obvious, showing that the droplet radius increases with optical thickness. Several authors [e.g., *Nakajima and Nakajima*, 1995; *Han et al.*, 1998; *Szczodrak et al.*, 2001] have shown that optically thin water clouds (with optical thickness lower than 15) over the ocean tend to have a positive correlation between effective droplet radius and optical thickness. This allowed us to reduce the number of parameters to be retrieved, assuming that the linear relationship determined from Figure 7 is also valid for the low cloud below the cirrus cloud. Finally, we also assumed that the lower cloud top temperature determined in a cirrus-free region can be used as an approximation of the nearby cirrus-covered

Figure 5. Correlations between ATSR-2 a) nadir 0.87 and 1.6 μm, b) nadir 0.87 and 3.7 μm and c) forward 0.87 and 1.6 μm channels for different ice particle effective diameters and habits. Following the curves from left to right the cirrus optical thickness increases, τ_i = 0.0, 0.125, 0.25, 0.5, ..., 32, 64. The cirrus top temperature is T_i = 235.0 K and the Sun-satellite geometry is (θ_0 = 63°, θ = 10° and $\Delta\phi$ = 113.5°) and (θ_0 = 63°, θ = 55° and $\Delta\phi$ = 164.5°) for the nadir and forward views respectively.
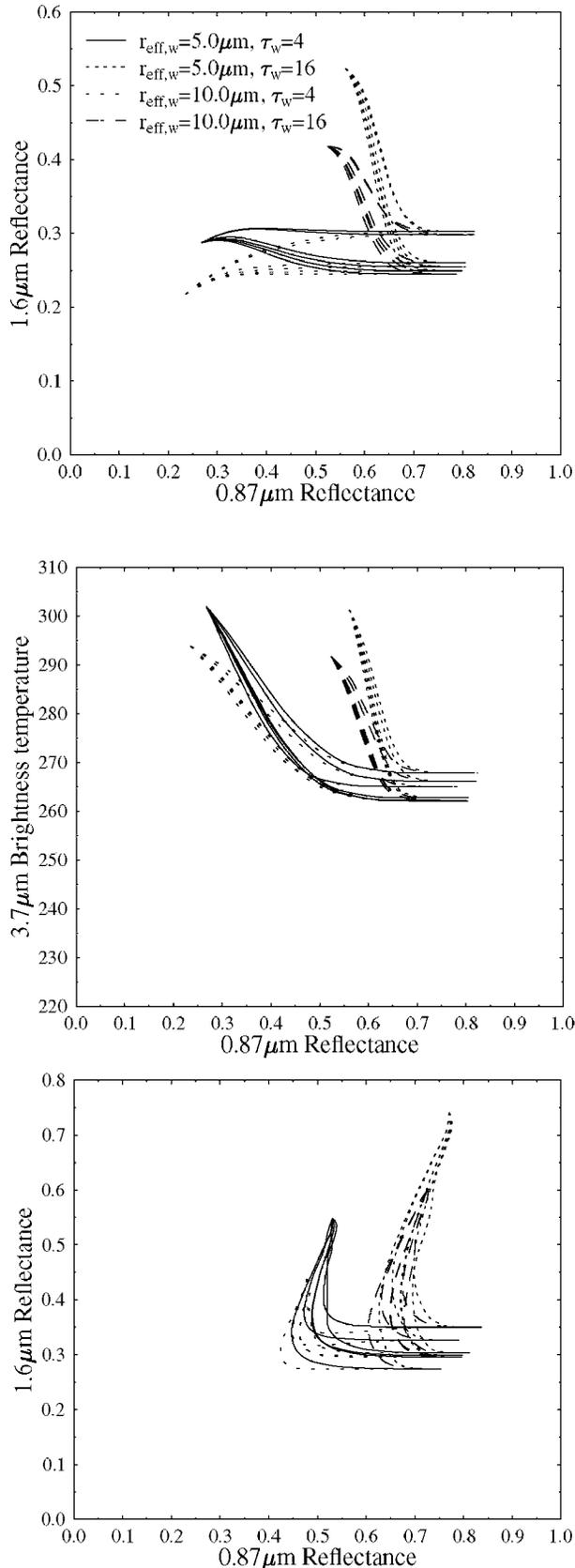
region. It is important to note that Figures 1a and 7 show a high variability of the reflectivity of the low water cloud which must be taken into account in the retrieval. In our retrieval this variability is expressed in terms of the low cloud optical thickness and implicitly in terms of the effective radius which is a function of the optical thickness.

[23] Finally, we end up with five parameters to be included in the retrieval: The desired cirrus parameters (effective diameter $D_{eff,i}$, predominant habit, optical thickness $\tau_{i,}$ and top temperature or altitude) and the optical thickness of the low water cloud τ_w. These five parameters are retrieved from five satellite radiances, the 0.87 μm and 1.6 μm nadir and forward observations and the 3.7 μm nadir observation. Since the radiative transfer model cannot be

inverted analytically, a least squares fitting technique was applied which allowed us to determine the desired parameters using the precalculated lookup table. A cost function was defined that accounts for the difference between the theoretical reflectances and temperatures and those measured by the radiometer onboard the satellite [*Nakajima and King*, 1990]:

$$cost = \sum_{i \in A} \left(R_{\text{model},i} - R_{satellite,i}\right)^2 + \alpha\left(T_{\text{model},3.7} - T_{satellite,3.7}\right)^2$$

(6)

where A = {0.87 μm nadir, 0.87 μm forward, 1.6 μm nadir, 1.6 μm forward}, $R_{model,i}$ is the theoretical reflectance for

channel i, computed for a particular set of low and high cloud parameters, $T_{model,3.7}$ is the corresponding brightness temperature for channel 3.7 μm. $R_{satellite,i}$ and $T_{satellite,i}$ are the observed reflectances and brightness temperature, which were averaged over 3×3 pixels to lower the effect of horizontal inhomogeneity [*Watts et al.*, 1998]. The parameter α is a factor to normalize the brightness temperature differences to differences in reflectances. For every pixel in the image the retrieved parameters are those that minimize the cost function in a five dimensional space.

[24] As a consequence of the large range of possible values for every parameter and their independence, the defined cost function has several local minima. For this reason, methods based on the Jacobian matrix are not appropriate to search for the global minimum in this case because their final solution depends on the initial trial point. Instead, methods are required which are insensitive to these local extremes such as annealing procedures [*Press et al.*, 1992], Montecarlo methods, genetic algorithms or scatter search. Genetic algorithms and scatter search have been applied successfully to stratocumulus parameters retrieval from NOAA-AVHRR data [*Pérez et al.*, 2000; *González et al.*, 2002]. Here we decided to use the scatter search method because it is faster.

[25] The scatter search method [*Glover et al.*, 2001] is an evolutionary procedure that operates on a set of solutions, named the reference set (relatively small in comparison with the "population" in genetic algorithms), systematically choosing two elements of it to create new solutions. The starting set of solutions is generated using a controlled randomization, distributing them all around the space of solutions. A heuristic process, based on a simplex method [*Nelder and Mead*, 1965] is applied to improve these solutions. Then, a collection of the best-improved solutions is selected and the next iteration step starts. The notion of best solution is broader than in the genetic algorithm method because not only "high quality" solutions (those
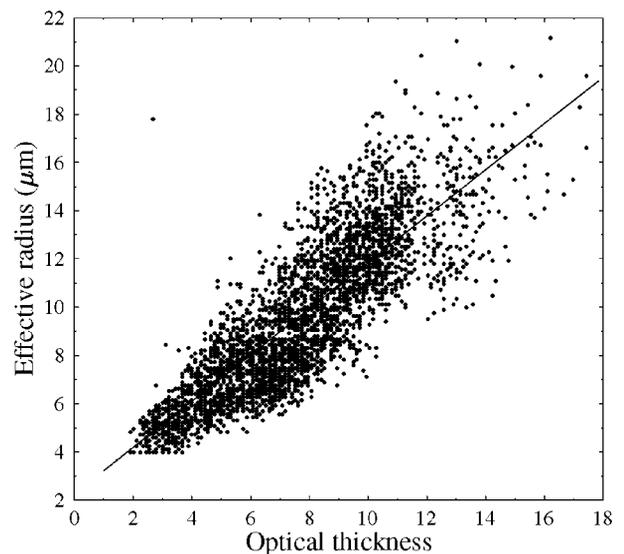

Figure 6. The same correlations as in Figure 5 but for different lower cloud droplet effective radii and optical thicknesses and assuming hexagonal columns as the cirrus cloud particle habit.

Figure 7. Correlation between the satellite retrieved effective droplet radius of the lower cloud and its optical thickness for the cirrus-free pixels of the box denoted in Figure 1b. The linear fit is $r_{eff,w} = 2.26 + 0.96\ \tau_w$.
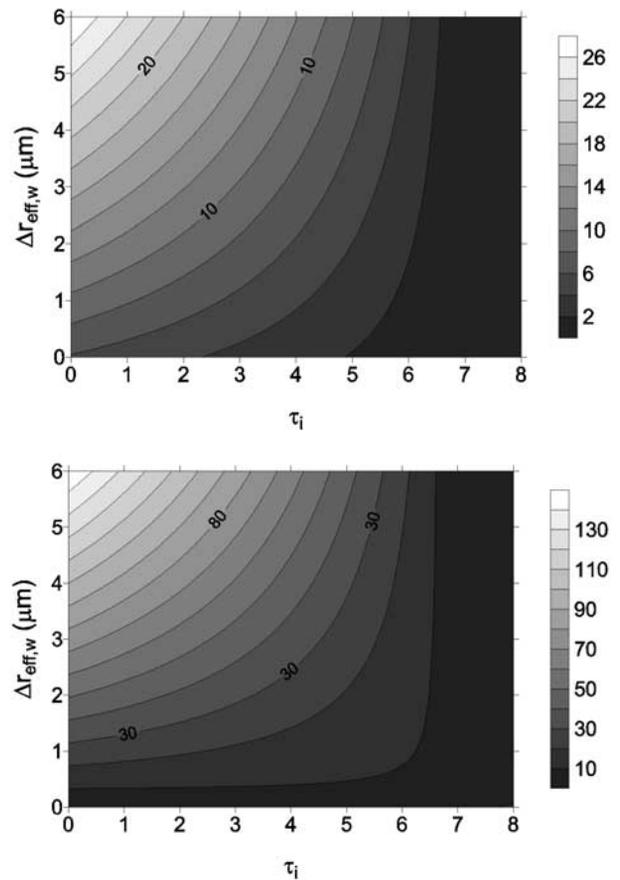
that provide lowest values for the cost function), but also "diverse solutions" (those whose Euclidean distances are furthest away from high quality solutions) are chosen to generate the new population. The iteration stops when the reference set does not change anymore and when all the pairs of elements have already been used to generate new solutions. To interpolate between the values provided by the lookup table, a spline interpolation in a five-dimensional space is used.

5.   Uncertainty Estimates

[26]   Each retrieval process has several sources of uncertainty. Here we investigate the robustness of the retrieved parameters with respect to uncertainties of the observed radiances and the consequences of the assumptions required for the retrieval.
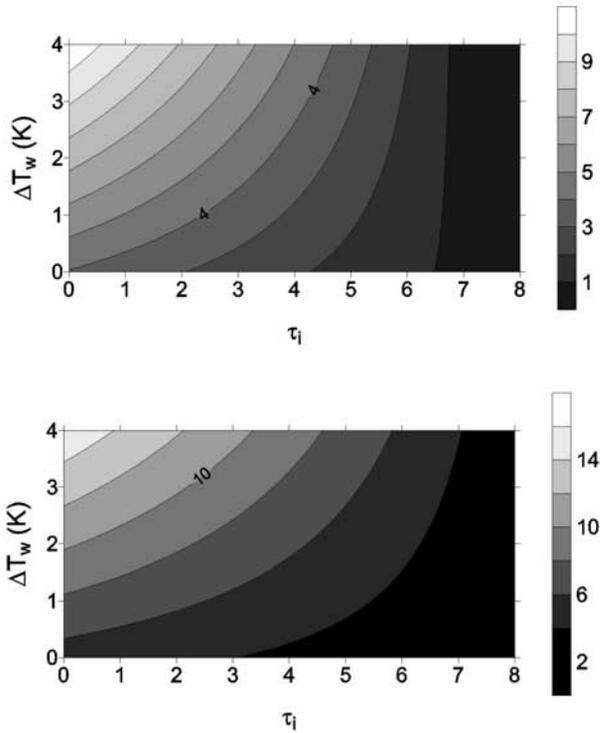
[27]   To check the existence of a unique global minimum of the cost function and to adjust the free parameters in the scatter search method (like population size or number of "high quality" and "diverse solutions"), numerous simulated cases, corresponding to different cloud conditions, have been used. Furthermore, small random errors have been applied to the simulated radiances, finding that the obtained parameters are very close to the actual solution. The method turned out to be robust, except for the cirrus cloud top temperature which is sensitive to uncertainties in the 3.7 μm channel brightness temperature for optically thin clouds. The reason is that the 3.7 μm brightness temperature is not only influenced by cloud top temperature but also, to a much larger degree, by other parameters, implying that a large change in cloud top temperature causes only a small change in brightness temperature. Or, vice versa, a small uncertainty in the brightness temperature may cause large uncertainties in the retrieved cloud top temperature. For this reason we do not report this parameter, although it is included in the retrieval scheme because it is required to separate the thin high cloud from the optically thick low cloud. The particle habit is also sensitive to radiance uncertainties, which is not surprising as the single scattering properties of some habits, like two- and three-dimensional rosettes, are nearly identical (see Figure 4). As a consequence, even from a theoretical point of view, habits with similar single scattering properties are not clearly separated by the retrieval. In the case of retrieving cloud parameters from real satellite data, the estimation of the predominant habit is even more complicated because most optically thin cirrus clouds contain a variety of complex habits which vary with altitude. In addition, as the radiances at 1.6 and 3.7 μm suffer different absorption by ice crystals the retrieved size in both channels could correspond to different physical depths in the cloud. Furthermore, the *Key et al.* [2002] parameterization is based in randomly orientation condition for ice crystals, but the orientation effect may be larger than the one associated with habit. Despite these facts we decided to keep the particle habit as a free retrieval parameter because it covers the range of phase functions to be expected from nonspherical particles which is an important prerequisite for the retrieval to work properly.

[28]   In addition to the determination of the errors in the retrieved parameters due to uncertainties in the observed radiances, it is necessary to consider the effects of the

Figure 8.   Percentage error in a) cirrus particle effective diameter and b) optical thickness due to uncertainties in low cloud effective droplet radius ($\Delta r_{eff,w}$) for different cirrus optical thicknesses (τ_i). The ice particles are solid columns with an effective diameter of 70 μm and the ice cloud temperature is assumed to be $T_i = 235.0$ K.

assumptions that are made by the retrieval, like the relationship between lower cloud particle size and optical thickness or the assumption of a constant lower cloud top temperature. Figure 8 presents the relative error of the retrieved cirrus particle effective diameter and optical thickness due to uncertainties $\Delta r_{eff,w}$ in the effective radius of the water cloud droplets, as a function of the cirrus cloud optical thickness τ_i. Such uncertainties arise due to the assumption of a linear relationship between $r_{eff,w}$ and τ_w described in the previous section. Figure 7 shows that the water cloud effective radius may deviate by several microns from the idealized linear approximation. The error estimates have been derived for a cirrus layer with top temperature $T_i = 235$ K composed of solid columns with an effective particle diameter $D_{eff,i} = 70$ μm, and for a lower water cloud with top temperature $T_w = 280$ K and optical thickness ranging from 0 to 32. The values shown in Figure 8 were obtained averaging the uncertainties over different optical thicknesses of the lower cloud. The largest errors occur, of course, for optically thin cirrus clouds. In this case, the satellite measurements are highly influenced by the radiance reflected at lower layers and hence are very sensitive to uncertainties in the microphysics of the low cloud.

Figure 9. Percentage error in a) cirrus particle effective diameter and b) optical thickness due to uncertainties in the low cloud temperature (ΔT_w) for different cirrus optical thicknesses (τ_i). The ice particles are solid columns with an effective diameter of 70 μm and the ice cloud temperature is assumed to be $T_i = 235.0$ K.

[29] Figure 9 shows the errors caused by uncertainties ΔT_w in the water cloud top temperature which were computed for the same cloud properties as in the previous case. Here the errors are much smaller, because the lower cloud temperature does not influence the 0.87 and 1.6 μm radiances but only the 3.7 μm channel brightness temperature. Uncertainties in the sea surface temperature estimate affect the retrieved values in a similar way, but its effect is only important when the lower layer is very thin or it is not present.
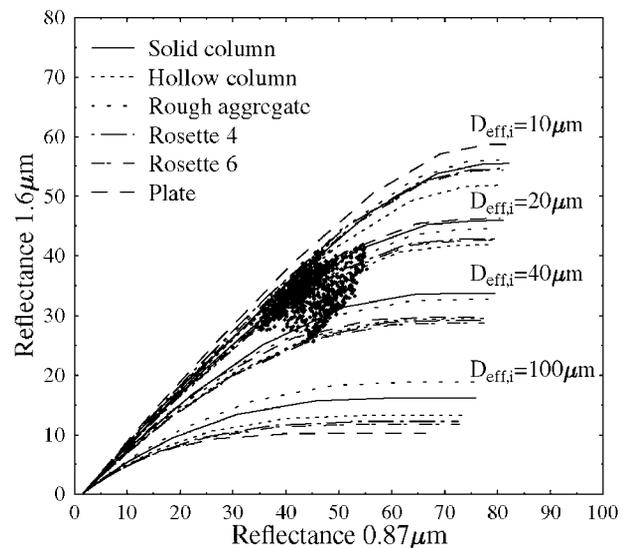
6. Comparison With Observations

[30] The retrieval scheme presented in section 4 was applied to the three boxes in Figure 1. Figure 10 shows an example of the relationship between the 0.87 and 1.6 μm reflectances for the six habits and for four different particle effective sizes. Satellite observations from leg 1 are superimposed as dots. Comparing these data with Figures 5a and 6a, it is obvious that the observations can be either explained by a single-layer cirrus cloud with small particles and large optical thickness or by an optically thin cirrus layer with larger particles overlying a water cloud. This is the reason for including the 3.7 μm channel in the retrieval because it removes the ambiguities and allows us to distinguish between the two possibilities.

[31] Results for the three boxes are presented in Tables 2 and 3. The cirrus cloud optical thickness is very small

compared to that of the low water cloud, and yet both are clearly separated by the retrieval. As an illustration, Figure 11 shows the histograms of high and low cloud retrieved optical thickness for leg 1. The best agreement between in situ measured and retrieved ice particle size is observed for leg 1. This is due to the fact that, for optically thin clouds, the satellite retrieval yields the vertically averaged mean effective ice crystal size, and leg 1 corresponds to an ascent of the Falcon within the cloud for which reason the averaged aircraft data correspond to a vertical average. Measurements for the other two legs were carried out at constant altitude and hence are not representative of the whole cloud. For leg 1, the cloud geometric thickness was inferred from Falcon observations and from notes taken by the pilots. A value of 2.2 km was obtained which, together with the in situ observed extinction of 0.25km^{-1}, corresponds to a visible optical thickness of 0.55. This value agrees well with the satellite retrieved optical thickness of 0.5, shown in Table 2.

[32] During leg 2, the aircraft ascended to the top of a thicker part of the cloud, which is reflected in the Falcon data and in the retrieved cirrus optical thickness and top temperature (Table 2). A decrease in particle size was observed during the ascent, for which reason the in situ effective size (observed around cloud top) is smaller than the value obtained from ATSR-2 data (averaged over altitude). Similar conditions occurred in leg 3. This fact indicates that due to the vertical inhomogeneity of cirrus clouds, multiple flight level data must be obtained to perform validation studies [see also, e.g., *Rolland et al.*, 2000].

Figure 10. An example of the correlation between 0.87 and 1.6 μm reflectances. The lines correspond to a variation of cirrus cloud optical thickness for different ice particle effective diameters and habits. Cirrus top temperature is $T_i = 235.0$ K and the Sun-satellite geometry is ($\theta_0 = 65.4°$, $\theta = 14.5°$ and $\Delta\phi = 132.0°$) and ($\theta_0 = 65.6°$, $\theta = 53.7°$ and $\Delta\phi = 165.0°$) for nadir and forward views respectively. The observed reflectances for the box corresponding to leg 1 are plotted as dots.

Table 2. Retrieved Mean Cirrus Effective Crystal Size, Optical Thickness, Temperature, Low Cloud Optical Thickness, and Associated Standard Deviations (in Parentheses) for the Three Boxes Used in this Study, Referenced as the Corresponding Legs
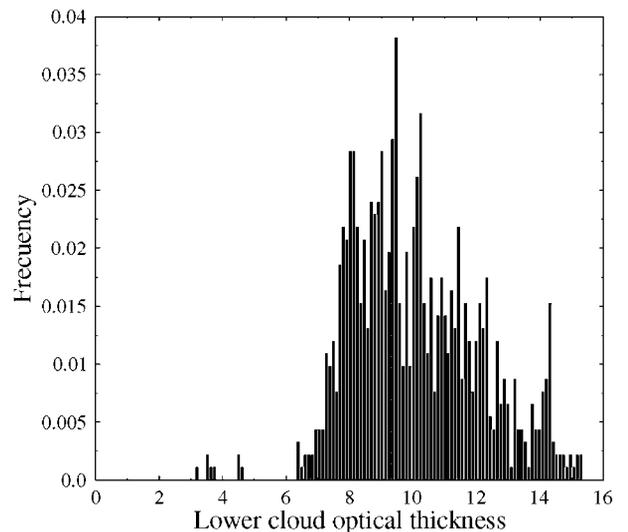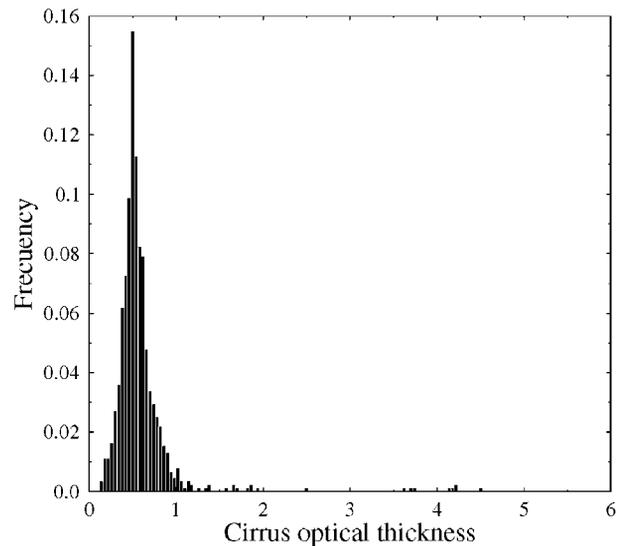
	Cirrus Cloud			Low Cloud
	$D_{\text{eff},i}$, μm	Optical Thickness	Temperature, K	Optical Thickness
Leg 1	54.7 (19.9)	0.5 (0.3)	230.1 (9.5)	10.1 (2.1)
Leg 2	51.4 (10.1)	1.2 (0.4)	220.4 (8.5)	4.2 (1.6)
Leg 3	56.4 (14.9)	0.7 (0.2)	227.9 (8.4)	8.1 (1.2)

[33] The ice particle habit is expressed in terms of the percentage of pixels in each box that correspond to this habit (Table 3). Due to the uncertainties exposed in the previous section, the interpretation of these results is more complicated. Moreover, the particle shape recognition from in situ measurements is not reliable for particles with diameters smaller than 150 μm due to the 2D-C probe pixel resolution. For these reasons the capability of the algorithm to estimate the particle habit cannot be validated by comparison with in situ data. In any case, the inclusion of the habit in the retrieval prevents possible larger errors in the other parameters, caused by an inadequate choice of a particular habit. In order to check these errors, the retrieval procedure has been applied to leg 1 case but assuming different a priori particle shapes. The results are shown in Table 4 for the six habits included in the *Key et al.* [2002] parameterization. In this particular case, the largest error in the retrieved ice particle effective diameter (12 μm) is found for the rough-aggregate habit. For solid columns and plates, the deviation in the optical thickness may reach a factor of 2.

[34] In the following it is demonstrated that the variability of the low cloud needs to be taken into account if the properties of the high clouds are to be retrieved with reasonable accuracy. As explained in section 4, our retrieval scheme automatically considers the pixel-to-pixel variability of the lower cloud optical thickness, and implicitly also of the effective radius. In Table 5, results for three different scenarios are presented: (a) the retrieval scheme as described above; (b) same as (a), but assumption of constant lower cloud optical properties where these were determined from a nearby cirrus-free region; and (c) same as (a) but without consideration of a lower cloud. It is obvious that the results are completely meaningless if the water cloud is neglected (scenario c); here the optical thickness is too large by a factor of 10 and also the effective diameter is off by a factor of 2. Also in the case when a lower cloud is considered and only its variability is neglected (scenario b), the results are considerably different from the full retrieval (scenario a). In particular, the optical thickness is overestimated by a

Figure 11. Histogram of the retrieved high and low cloud optical thicknesses for all pixels in the box corresponding to flight leg 1.

factor of 3. The ice particle size is less sensitive to the assumption of a constant water cloud than the optical thickness. These results clearly illustrate the need to consider not only the lower cloud but also its variability.

7. Summary and Conclusions

[35] A new retrieval was proposed, combining three channels of the ATSR-2 instrument in two viewing geo-

Table 3. Percentage of Pixels in the Three Boxes Labeled as Containing a Particular Predominant Habit After Retrieval Application

	Solid Column, %	Hollow Column, %	Rough Aggregate, %	Rosette-4, %	Rosette-6, %	Plate, %
Leg 1	14.4	42.4	6.2	23.7	7.7	5.6
Leg 2	53.4	4.5	0.1	35.3	3.9	2.8
Leg 3	20.7	29.4	0.2	44.0	2.1	3.6

Table 4. Comparison Between Retrieved Values for Leg 1 Assuming Different A Priori Crystal Habits

	Solid Column	Hollow Column	Rough Aggregate	Rosette-4	Rosette-6	Plate
$D_{\text{eff},i}$, μm	57.8	56.2	67.2	53.1	53.0	52.2
Optical thickness	1.1	0.5	0.5	0.6	0.6	0.9

Table 5. Comparison Between Retrieved Values for Leg 1 Assuming Different Conditions for the Lower Cloud: Variable, Constant, and Without a Lower (Water) Cloud

Variable Lower Cloud		Constant Lower Cloud		Without Lower Cloud	
$D_{eff,i}$, μm	Optical Thickness	$D_{eff,i}$, μm	Optical Thickness	$D_{eff,i}$, μm	Optical Thickness
54.7	0.5	47.6	1.6	25.8	6.14

metries. The retrieval allows the separation of optically thin cirrus clouds from underlying water clouds as has been confirmed by a comparison with in situ observations. In this way, it is possible to determine optical thickness and effective particle size of cirrus clouds even with the presence of lower clouds. A case study has shown the importance of considering the pixel-to-pixel variability of the low cloud; neglecting the variability of the low cloud may cause significant systematic errors in the retrieved cirrus cloud optical properties. The combination of five ATSR-2 observations, the nadir 0.87, 1.6 and 3.7 μm channels and the 0.87 and 1.6 μm forward channels permits the retrieval of cirrus particle size, optical thickness and top temperature, and lower cloud optical thickness. A sensitivity study showed that all retrieved parameters are numerically robust, except the cloud top height of the optically thin cirrus. The particle habit is not a robust retrieval parameter but it has been included in the retrieval to avoid errors in the other retrieved parameters due to an inadequate selection of a particular habit. The use of the ice cloud parameterization by *Key et al.* [2002] simplifies the radiative transfer simulation of satellite observations for various cloud conditions and viewing geometries. Nevertheless, the use of the double Henyey-Greenstein function to approximate the scattering phase functions may artificially diminish the differences between several particle habits as it does not properly reproduce special features of the phase function occurring for some habits, e.g. the halos typical of hexagonal columns. This fact makes the determination of the dominating ice particle shape more uncertain. However, the volumetric scattering cross-sections measured in situ by the polar nephelometer support the idea of using the proposed featureless approximated phase functions because the typical halos for hexagonal particles were not present in the observation. On the other hand, the theoretical computations underestimate the backscattering peak of the observed phase function, making further studies necessary to explain these deviations. In any case, it is obvious from this comparison that the phase function for spherical particles is significantly different from that of nonspherical particles (observed as well as calculated) preventing the use of Mie theory to calculate the single scattering properties of cirrus clouds.

[36] In order to invert the radiative transfer model, five-dimensional lookup tables were created. An evolutionary procedure called scatter search was utilized to find the global minimum of the defined cost function, which takes into account the differences between theoretically calculated and observed reflectances and brightness temperatures. This method provides a simple way to change the radiometer bands included in the cost function without modifying the global retrieval scheme, thus facilitating sensitivity studies to determine the optimum combination of observations to derive the desired parameters.

[37] The analysis of retrieved and in situ observed cirrus parameters suggests that the aircraft measurements must provide profiles of the optical properties by making observations in multiple in-cloud levels because otherwise the in situ observations are not representative of the whole cloud. In our case, this is only true for the first of the three legs analyzed in this paper. Consequently, the agreement is best for this leg. Although the presented study shows reasonable agreement with in situ observations, further studies covering a much larger sample of observations are required to fully validate the method.

References

Anderson, G. P., S. A. Clough, F. X. Kneizys, J. H. Chetwynd, and E. P. Shettle, AFGL atmospheric constituent profiles (0–120 km), *AFGL Tech. Rep. AFGL-TR-86-0100*, Hanscom Airforce Base, Mass., 1986.

Arnott, W. P., Y. Y. Dong, and J. Hallet, Role of small ice crystals in radiative properties of cirrus: A case study, FIRE II, November 22, 1991, *J. Geophys. Res.*, 99, 1371–1381, 1994.

Auriol, F., J. F. Gayet, G. Febvre, O. Jourdan, L. Labonnotte, and G. Brogniez, In situ observations of cirrus cloud scattering phase function with 22° and 46° halos: Cloud field study on 19 February 1998, *J. Atmos. Sci.*, 58, 3376–3390, 2001.

Baran, A. J., S. J. Brown, J. S. Foot, and D. L. Mitchell, Retrieval of tropical cirrus thermal optical depth, crystal size and shape using a dual-view instrument at 3.7 and 10.8 μm, *J. Atmos. Sci.*, 56, 92–110, 1999a.

Baran, A. J., P. D. Watts, and P. N. Francis, Testing the coherence of cirrus microphysical and bulk properties retrieved from dual-viewing multispectral satellite radiance measurements, *J. Geophys. Res.*, 104, 31,673–31,683, 1999b.

Baum, B. A., and J. D. Spinhirne, Remote sensing of cloud properties using MODIS Airborne Simulator imagery during SUCCESS, 3, Cloud overlap, *J. Geophys. Res.*, 105, 11,793–11,804, 2000.

Baum, B. A., R. F. Arduini, B. A. Wielicki, P. Minnis, and S.-C. Tsay, Multilevel cloud retrieval using multispectral HIRS and AVHRR data: Nighttime oceanic analysis, *J. Geophys. Res.*, 99, 5499–5514, 1994.

Baum, B. A., T. Uttal, M. Poellot, T. P. Ackerman, J. M. Alvarez, J. Intrieri, D. O'C. Starr, J. Titlow, V. Tovinkere, and E. Clothiaux, Satellite remote sensing of multiple cloud layers, *J. Atmos. Sci.*, 52, 4210–4230, 1995.

Baum, B. A., V. Tovinkere, J. Titlow, and R. M. Welch, Automated cloud classification of global AVHRR data using a fuzzy logic approach, *J. Appl. Meteorol.*, 36, 1519–1540, 1997.

Baumgardner, D., J. E. Dye, R. G. Knollenberg, and B. W. Gandrud, Interpretation of measurements made by the FSSP-300X during the Airborne Artic Stratospheric Expedition, *J. Geophys. Res.*, 97, 8035–8046, 1992.

Crépel, O., J. F. Gayet, J. F. Fournol, and S. Oshchepkov, A new airborne polar Nephelometer for the measurements of the optical and microphysical cloud properties, 2, Preliminary tests, *Ann. Geophys.*, 15, 460–470, 1997.

Doutriaux-Boucher, M., J. C. Buriez, G. Brogniez, L. C. Labonnote, and A. J. Baran, Sensitivity of retrieved POLDER directional cloud optical thickness to various ice particle models, *Geophys. Res. Lett.*, 27, 109–112, 2000.

Fu, Q., W. B. Sun, and P. Yang, Modeling of scattering and absorption by nonspherical cirrus ice particles at thermal infrared wavelengths, *J. Atmos. Sci.*, 56, 2937–2947, 1999.

Gayet, J. F., G. Febvre, G. Brogniez, H. Chepfer, W. Renger, and P. Wendling, Microphysical and optical properties of cirrus and contrails: Cloud field study on 13 October 1989, *J. Atmos. Sci.*, *53*, 126–138, 1996.

Gayet, J. F., O. Crépel, J. F. Fournol, and S. Oshchepkov, A new airborne polar Nephelometer for the measurements of the optical and microphysical cloud properties, 1, Theoretical design, *Ann. Geophys.*, *15*, 451–459, 1997.

Gayet, J. F., F. Auriol, S. Oshchepkov, F. Schröder, C. Duroure, G. Febvre, J. F. Fournol, O. Crépel, P. Personne, and D. Daugeron, In situ measurements of the scattering phase function of stratocumulus, contrails and cirrus, *Geophys. Res. Lett.*, *25*, 971–974, 1998.

Glover, F., M. Laguna, and R. Martí, *Theory and Applications of Evolutionary Computation: Recent Trends*, edited by A. Ghosh and S. Tsutsui, Springer-Verlag, New York, in press, 2001.

González, A., J. C. Pérez, F. Herrera, F. Rosa, M. A. Wetzel, R. D. Borys, and D. H. Lowenthal, Stratocumulus properties retrieval method from NOAA-AVHRR data based on the discretization of cloud parameters, *Int. J. Remote Sens.*, *23*, 627–645, 2002.

Han, Q., W. B. Rossow, J. Chou, and R. M. Welch, Global survey of the relationships of cloud albedo and liquid water path with droplet size using ISCCP, *J. Clim.*, *11*, 1516–1528, 1998.

Hess, M., and M. Wiegner, COP: A data library of optical properties of hexagonal ice crystals, *Appl. Opt.*, *33*, 7740–7746, 1994.

Heymsfield, A. J., Ice crystal terminal velocities, *J. Atmos. Sci.*, *29*, 1348–1357, 1972.

Heymsfield, A. J., and C. M. R. Platt, A parameterization of the particle size spectrum of ice clouds in terms of the ambient temperature and ice water content, *J. Atmos. Sci.*, *41*, 846–856, 1984.

Key, J., P. Yang, B. Baum, and S. Nasiri, Parameterization of shortwave ice cloud optical properties for various particle habits, *J. Geophys. Res.*, *107*(D13), 4181, doi:10.1029/2001JD000742, 2002.

King, M. D., S. C. Tsay, S. E. Platnick, M. Wang, and K. N. Liou, Cloud retrieval algorithms for MODIS: Optical thickness, effective particle radius and thermodynamic phase, in *MODIS Algorithm Theoretical Basis Doc. ATBD-MOD-05 MOD-06-Cloud Product*, 79 pp., NASA Goddard Space Flight Cent., Greenbelt, Md., 1997.

Knap, W. H., M. Hess, P. Stammes, and R. B. A. Koelemeijer, Cirrus optical thickness and crystal size retrieval from ATSR-2 data using phase functions of imperfect hexagonal ice crystals, *J. Geophys. Res.*, *104*, 31,721–31,730, 1999.

Knollenberg, R. G., Techniques for probing cloud microstructure, in *Clouds, Their Formation, Optical Properties and Effects*, edited by P. V. Hobbs and A. Deepak, pp. 15–92, Academic, San Diego, Calif., 1981.

Kylling, A., and B. Mayer, libRadtran, A package for radiative transfer calculations in the ultraviolet, visible, and infrared, 1993–2002 .

Liou, K. N., Influence of cirrus clouds on weather and climate processes: A global perspective, *Mon. Weather Rev.*, *114*, 1167–1199, 1986.

Liou, K. N., *Radiation and Cloud Processes in the Atmosphere*, 487 pp., Oxford Univ. Press, New York, 1992.

Locatelli, J. D., and P. V. Hobbs, Fall speeds and masses of solid precipitation particles, *J. Geophys. Res.*, *79*, 2185–2197, 1979.

Mace, G. G., T. P. Ackerman, and E. E. Clothiaux, A study of composite cirrus morphology using data from a 94-GHz radar and correlation with temperature and large-scale vertival motion, *J. Geophys. Res.*, *102*, 13,581–13,593, 1997.

Macke, A., Scattering of light by polyhedral ice crystals, *Appl. Opt.*, *32*, 2780–2788, 1993.

Macke, A., J. Mueller, and E. Raschke, Single scattering properties of atmospheric ice crystals, *J. Atmos. Sci.*, *53*, 2813–2825, 1996.

McFarquhar, G. M., and A. J. Heymsfield, Parameterization of tropical cirrus ice crystal size distributions and implications for radiative transfer: Results from CEPEX, *J. Atmos. Sci.*, *54*, 2187–2200, 1997.

McFarquhar, G. M., A. J. Heymsfield, A. Macke, J. Iaquinta, and S. M. Aulenbach, Use of observed ice crystal sizes and shapes to calculate mean-scattering properties and multispectral radiances: CEPEX April 4, 1993, case study, *J. Geophys. Res.*, *104*, 31,763–31,779, 1999.

Mishchenko, M., W. Rossow, A. Macke, and A. A. Lacis, Sensitivity of cirrus cloud albedo, bi-directional reflectance and optical thickness retrieval accuracy to ice particle shape, *J. Geophys. Res.*, *101*, 16,973–16,985, 1996.

Mitchell, D. L., and W. P. Arnott, A model predicting the evolution of ice particles size spectra and radiative properties of cirrus clouds, 2, Dependence of absorption and extinction on ice crystal morphology, *J. Atmos. Sci.*, *51*, 817–832, 1994.

Nakajima, T., and M. D. King, Determination of the optical thickness and effective particle radius of clouds from reflected solar radiation measurements, 1, Theory, *J. Atmos. Sci.*, *47*, 1878–1893, 1990.

Nakajima, T. Y., and T. Nakajima, Wide-area determination of cloud microphysical properties from NOAA AVHRR measurements for FIRE and ASTEX regions, *J. Atmos. Sci.*, *52*, 4043–4059, 1995.

Nelder, J. A., and R. Mead, A simplex method for function minimisation, *Comput. J.*, *7*, 308–313, 1965.

Nicolet, M., On the molecular scattering in the terrestrial atmosphere: An empirical formula for its calculation in the homosphere, *Planet. Space Sci.*, *32*, 1467–1468, 1984.

Ou, S. C., K. N. Liou, W. M. Gooch, and Y. Takano, Remote sensing of cirrus cloud parameters using advanced very-high-resolution radiometer 3.7- and 10.0-μm channels, *Appl. Opt.*, *32*, 2171–2180, 1993.

Ou, S. C., K. N. Liou, and B. A. Baum, Detection of multilayer cirrus cloud systems using AVHRR data: Verification based on FIRE-II IFO composite measurements, *J. Appl. Meteorol.*, *35*, 178–191, 1996.

Ou, S. C., K. N. Liou, and T. Caudill, Remote sounding of multilayer cirrus cloud systems using AVHRR data collected during FIRE-II-IFO, *J. Appl. Meteorol.*, *37*, 241–254, 1998.

Ou, S. C., K. N. Liou, M. D. King, and S. C. Tsay, Remote sensing of cirrus cloud parameters based on a 0.63–3.7 μm radiance correlation technique applied to AVHRR data, *Geophys. Res. Lett.*, *26*, 2439–2440, 1999.

Pérez, J. C., F. Herrera, F. Rosa, and A. González, Stratocumulus parameters retrieval using MODIS nighttime imagery: A theoretical approach, paper presented at the International Symposium on Remote Sensing (SPIE-EUROPTO), Barcelona, Spain, 25–29 September, 2000.

Prata, A. J. F., R. P. Cechet, I. J. Barton, and D. T. Llewellyn-Jones, The Along-Track Scanning Radiometer (ATSR) for ERS-1: Scan geometry and data simulation, *IEEE Trans. Geosci. Remote Sens.*, *28*, 3–13, 1990.

Press, W. H., S. A. Teukolsky, W. T. Vetterling, B. T. Flannery, *Numerical Recipies in C: The Art of Scientific Computing*, Cambridge Univ. Press, New York, 1992.

Ramanathan, V., R. D. Cess, E. F. Harrison, P. Minnis, B. R. Backstrom, E. Ahmad, and D. Hartmann, Cloud-radiative forcing and climate: Results from the Earth Radiation Budget Experiment, *Science*, *243*, 57–63, 1989.

Raschke, E., J. Schmetz, J. Heintzenberg, R. Kandel, and R. Saunders, The International Cirrus Experiment (ICE)—A joint European effort, *ESA J.*, *4*, 193–199, 1990.

Ricchiazzi, P., S. Yang, C. Gautier, and D. Sowie, SBDART: A research and teaching software tool for plane-parallel radiative transfer in the Earth's atmosphere, *Bull. Am. Meteorol. Soc.*, *79*, 2101–2114, 1998.

Rolland, P., K. N. Liou, M. D. King, S. C. Tsay, and G. M. McFarquhar, Remote sensing of optical and microphysical properties of cirrus clouds using Moderate-Resolution Imaging Spectroradiometer channels: Methodology and sensitivity to physical assumptions, *J. Geophys. Res.*, *105*, 11,721–11,738, 2000.

Rother, T., Generalization of the separation of variables method for nonspherical scattering on dielectric objects, *J. Quant. Spectrosc. Radiat. Transfer*, *60*, 335–353, 1998.

Rother, T., S. Havemann, and K. Schmidt, Scattering of plane waves on finite cylinders with noncircular cross sections, in *Progress in Electromagnetics Research (PIER)*, vol. 23, edited by J. A. Kongs, pp. 79–105, EMW, Cambridge, Mass., 1999.

Rother, T., K. Schmidt, and S. Havemann, Light scattering on hexagonal ice columns, *J. Opt. Soc. Am.*, *18*, 2512–2517, 2001.

Sauvage, L., H. Chepfer, V. Trouillet, P. H. Flamant, G. Brogniez, J. Pelon, and F. Albers, Remote sensing of cirrus parameters during EUCREX'94. Case study of 17 April 1994, 1, Observations, *Mon. Weather Rev.*, *127*, 486–503, 1999.

Sospedra, F., V. Caselles, and E. Valor, Effective wavenumber for thermal infrared bands—application to Landsat-TM, *Int. J. Remote Sens.*, *19*, 2105–2117, 1998.

Stamnes, K., D. Tsay, W. Wiscombe, and K. Jayaweera, Numerically stable algorithm for discrete-ordinate-method radiative transfer in multiple scattering and emitting layered media, *Appl. Opt.*, *27*, 2502–2509, 1988.

Starr, D. O'C., A cirrus intensive field observations for FIRE, *Bull. Am. Meteor. Soc.*, *68*, 119–124, 1987.

Stephens, G. L., S. C. Tsay, P. W. Stackhouse Jr., and P. J. Flatau, The relevance of the microphysical properties of cirrus clouds to climate and climatic feedback, *J. Atmos. Sci.*, *47*, 1742–1753, 1990.

Ström, J., et al., Aerosol and cirrus measurements at midlatitudes on the Southern hemisphere: An overview based on the first INCA experiment, *Air Pollut. Rep. 74*, *Rep. EUR 19,428 EN*, European Commission, Brussels, 2001.

Szczodrack, M., P. H. Austin, and P. B. Ktummel, Variability of optical depth and effective radius in marine stratocumulus clouds, *J. Atmos. Sci.*, *58*, 2912–2926, 2001.

Takano, Y., and K. N. Liou, Solar radiative transfer in cirrus clouds, 1, Single-scattering and optical properties of hexagonal ice crystals, *J. Atmos. Sci.*, *46*, 3–19, 1989.

Tian, L., and J. A. Curry, Cloud overlap statistics, *J. Geophys. Res.*, *94*, 9925–9935, 1989.

Viollier, M., Teledetection des concentrations de sestons et pigments chlorophylliens contenus dans l'Ocean, Ph.D. thesis, Ecole Polytechnique, Paris, 1980.

Volkovitskiy, O. A., L. N. Pavlova, and A. G. Petrushin, Scattering of light by ice crystals, *Atmos. Ocean Phys.*, 16, 90–102, 1980.

Watts, S. K., P. D. Watts, and A. J. Baran, Tropical cirrus cloud parameters from the Along Track Scanning Radiometer (ATSR-2), paper presented at the International Symposium on Remote Sensing (SPIE-EUROPTO), Barcelona, Spain, 21–24 September, 1998.

Wendling, P., R. Wendling, and H. K. Weickmann, Scattering of solar radiation by hexagonal ice crystals, *Appl. Opt.*, 18, 2663–2671, 1979.

Wiscombe, W., Improved Mie scattering algorithms, *Appl. Opt.*, 19, 1505–1509, 1980.

Yang, P., K. N. Liou, K. Wyser, and D. Mitchell, Parameterization of the scattering and absorption properties of individual ice crystals, *J. Geophys. Res.*, 105, 4699–4718, 2000.

Yang, P., B.-C. Gao, B. A. Baum, W. Wiscombe, Y. Hu, S. L. Nasiri, P. F. Soulen, A. J. Heymsfield, G. M. McFarquhar, and L. M. Miloshevich, Sensitivity of cirrus bidirectional reflectance at MODIS bands to vertical inhomogeneity of ice crystal habits and size distributions, *J. Geophys. Res.*, 106, 17,267–17,291, 2001.

_____

J.-F. Gayet, Laboratoire de Météorologie Physique/CNRS 6010, Université Blaise Pascal, 24, avenue des Landais, 63177 Aubiere, Cedex, France. (gayet@opgc.univ-bpclermont.fr)

A. González, Dpto. Física Fund. y Experimental, Electrónica y Sistemas, Universidad de La Laguna, 38023 La Laguna, Tenerife, Canary Islands, Spain. (aglezf@ull.es)

B. Mayer and P. Wendling, Institut für Physik der Atmosphäre, DLR, Oberpfaffenhofen, D-82234, Wessling, Germany. (Bernhard.Mayer@dlr.de; Peter.Wendling@dlr.de)

T. Rother, Institut für Methoden der Fernerkundung, DLR, Oberpfaffenhofen, D-82234 Wessling, Germany. (Tom.Rother@dlr.de)